

The Influence of Low Temperature on the Corrosion of EH40 Steel in a NaCl Solution

Yuanyuan Shen¹, Yaohua Dong^{2, 1, *}, Hengding Li¹, Xueting Chang¹, Dongsheng Wang¹,
Qinghong Li¹ and Yansheng Yin¹

¹ College of Ocean Science and Engineering, Shanghai Maritime University, Shanghai 201306, China;

² School of Mechanical Engineering, Shanghai Jiaotong University, Shanghai 200240, China

*E-mail: yhdong@shmtu.edu.cn

Received: 3 April 2018 / Accepted: 4 May 2018 / Published: 5 June 2018

The high strength ocean engineering structural steel EH40 exhibited great potential for the building of polar expedition ships due to high performance strength, relevant low-temperature impact toughness, prominent ship plate steel extensions, and outstanding weldability. The corrosion behavior of modified EH40 steel in low-temperature (0 °C) 3.5Wt% NaCl solution over a 56-day period was investigated using mass loss techniques, surface characterization, component analysis, and electrochemical measurements. The results showed that the corrosion rate of EH40 steel in low-temperature artificial seawater was relatively high compared to artificial seawater at room-temperature after 14 days of immersion. Notably, in the low-temperature NaCl solution, the scale deposits consisted mainly of Fe(Cl_xO_y) under which, corrosion pits were initiated. Moreover, uneven corrosion products formed on the steel surface and the size of the pit gradually increased with immersion time. In contrast, for the room temperature NaCl solution, a compact and thick corrosion product film covered the steel surfaces, protecting the steel from further corrosion and a characteristic uniform corrosion was present in the steel.

Keywords: EH40 steel; extreme cold environment; pitting corrosion; microstructure; EIS

1. INTRODUCTION

With the constant exploitation of land resources in recent years, some oil and gas resources are approaching depletion [1-5]. Consequently, there is an increased interest in oil and natural gas resources located in Arctic regions. According to an assessment conducted by the U.S. Geological Survey (USGS) [6-8], the Arctic holds an estimated 13% (90 billion barrels) of the world's undiscovered conventional oil resources and 30% of its undiscovered conventional natural gas resources. Considering the effects of permanent sea ice and oceanic water depth [9-11], the exploration

of the Arctic for petroleum and natural gas is deemed more technically challenging compared to other environments. However, recent technological developments [12] and relatively high oil prices have encouraged the petroleum and natural gas industries towards Arctic exploration.

One of the greatest challenges facing Arctic oil and natural gas deposit development is the required equipment, which is mainly composed of metal materials that need to withstand frigid temperatures [13-14]. For example, low temperature steel plays an important role in building special ships including liquefied natural gas (LNG) ships, liquefied petroleum gas (LPG) ships, and icebreakers [15-17]. At present, most countries (including China) consider ice shipbuilding as a priority research area. In China, the only ice vessel is the 1990's Ukrainian-built "Xue Long". Consequently, it is highly important to develop a novel low temperature steel for ice vessel building applications and to evaluate its corrosion behavior in extreme cold environments.

Chloride ions in seawater cause corrosion on metal materials. Previous work has investigated the anticorrosion behavior of carbon steel, aluminium alloy, and composite materials in seawater [18-20]. Although two properties, low-temperature toughness and high-efficiency welding process of EH40 steels, are currently being investigated [21-26], the effect of extremely cold seawater on the corrosion behavior of metallic materials has yet to be studied. Hydrogen-induced cracking of X70 pipeline steel in low-temperature and low-dissolved-oxygen seawater has been reported [27]. Less research was performed on the corrosion behavior of EH40 steel at low-temperature in seawater, which is partially due to the extremely cold environment, which causes the seawater to freeze. Consequently, it is hard to measure the immersion corrosion of metal at subzero degree temperatures.

In this work, 3.5% NaCl solutions at 0 °C (the temperature of the ice water mixture) and 25 °C (as the control) were selected as corrosive medium to observe and compare the corrosion behavior of EH40 steel. Understanding the corrosion behavior of the steel in extreme cold seawater and the influence of low-temperature on the corrosion process is imperative for the further development of materials used in extremely cold environments. Scanning electron microscopy (SEM) was used to observe the EH40 steel corrosion morphology in cooling solution. Other analytical techniques including energy dispersive spectrum (EDS) and X-ray diffraction (XRD) were employed to investigate the corrosion product components, and electrochemical impedance spectroscopy (EIS), polarization curve, and corrosion rate were used to explain the corrosion mechanism.

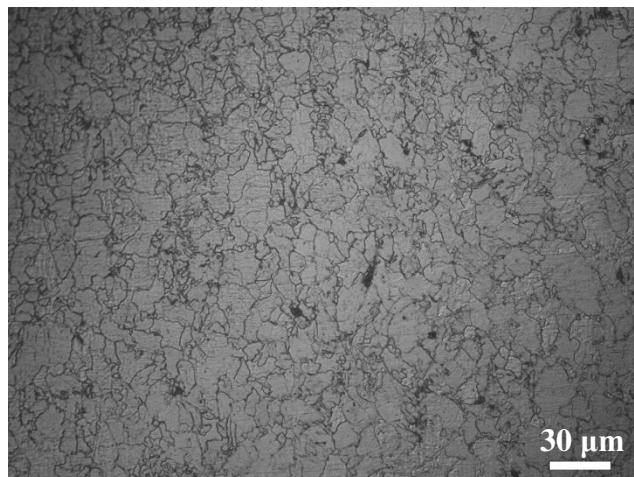
2. MATERIALS AND METHODS

2.1 Test Specimen and Preparations

Bao Steel supplied the modified high strength structural steel EH40 as a plate with planar dimensions of 300 × 500 mm and a thickness of 30 mm. Steel ingots were prepared using a vacuum furnace and the thickness was 250 mm. Table 1 lists the main chemical compositions. The ingots were rolled at 1443 K, reducing the ingot thickness from 250 mm to 30 mm. The resultant strip was furnace-cooled to 853 K, and then water-cooled to room temperature. The material base structure is predominantly ferrite and pearlite.

Table 1. Main composition of EH40 steels.

Element	P	S	C	Cr	Si	Mn	Mo	V	Ni	Nb	Ti	Al	Fe	Cu
Content (wt%)	< 0.010	< 0.0015	0.16	0.20	0.15	0.90	0.08	0.10	0.40	0.02	0.02	0.015	Bal.	0.35

**Figure 1.** Metallographic structure of EH40 steel.

Coupons (10 mm × 10 mm × 2 mm) were cut from the supplied steel plates and used for mass loss assays, electrochemical tests, and surface and component analyses. All specimens were ground to 800# using SiC paper, while electrochemical specimens were initially welded with copper wire, and then encapsulated with bare copper wire. The weld surface was encapsulated with ethoxyline resin. Prior to the experiments, the exposed surfaces of electrochemical samples were ground to 800# using SiC paper and the exposure area of electrochemical specimens was ensured to be 1 cm². All samples were then rinsed with deionized water and degreased with acetone for 2 min before drying under cool air. Afterwards, all samples were placed in a desiccator for 24 h. The coupon weights (for corrosion rate tests) were then measured using a precise electronic balance (Shanghai, China, FA 114).

2.2 Experimental Method

For this study, a cooling installation with a temperature control system was used. Figure 2 displays the system schematic. The temperature of refrigerating medium in the tank was maintained at 0 ± 0.1 °C and the vessel with artificial sea water (NaCl solutions with concentrations of 35 g/l ± 5 g/l) was placed into the tank with cooling medium. The temperature of the artificial sea water was also maintained at 0 ± 0.1 °C using heat transmission and was continuously measured during the experiments. The specimens for corrosion rate, electrochemical tests, and corrosion morphology analysis were immersed in the artificial sea water, were collected from the cold medium after 7, 14, 21, 28, 42, and 56 days of exposure, and then electrochemical measurements, surface analysis, and corrosion rate tests were performed. To create control experiments, the same steel specimens were exposed to the same NaCl medium at 25 °C.

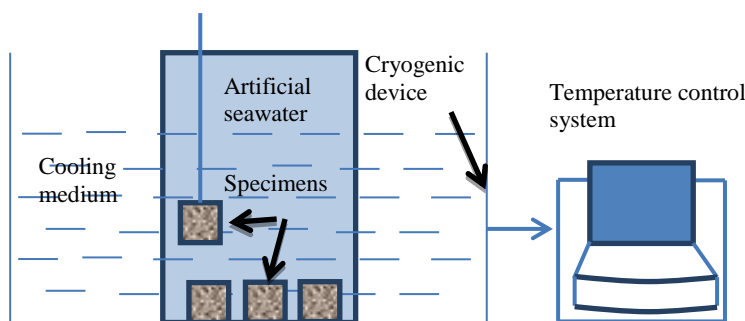


Figure 2. Schematic diagram of low-temperature immersion tests in artificial seawater.

2.3 Corrosion Rate

After immersion tests, the specimens were removed from the solution, cleaned with distilled water, and then the corrosion products were removed with a mixed solution (10% hydrochloric acid with 10 g/L hexamethylenetetramine) [28]. After corrosion product removal, the samples were rinsed with absolute ethyl alcohol and dried. Next, the specimens were weighed again to estimate the corrosion rate. The corrosion rate was calculated by the following formula:

$$V_{\text{corr}} = \Delta m / (S \cdot t), \quad (1)$$

Where V_{corr} is the corrosion rate in $\text{mg} \cdot \text{dm}^{-2} \cdot \text{d}^{-1}$, Δm is the weight loss in g, S is the surface area of the specimen in dm^2 , and t is the corrosion time in days (d). Triplicate specimens were used to calculate the corrosion rate after exposure in solution for different times.

2.4 Electrochemical Measurements

For electrochemical measurements, a conventional three-electrode glass corrosion cell was used. A saturated calomel electrode (SCE) was the reference electrode, a platinum sheet with an area of 1 cm^2 was used as the counter electrode, and the low-temperature steel sample immersed for different times served as the working electrode. Before EIS experiments, the open circuit potential (OCP) of specimens over time was tested for at least 30 min to guarantee the stability of the test procedure. EIS experiments were conducted within a frequency range of 10^4 Hz to 10^{-2} Hz versus OCP with a voltage perturbation of $\pm 5 \text{ mV}$. Tafel plots were recorded at a scan rate of 1 mV/s ranging from -250 to 250 mV at the OCP to determine the corrosion current density (i_{corr}) and the corrosion potentials (E_{corr}).

2.5 Surface topography and chemical analysis

Morphologies of the corrosion product formed on the alloy surface and morphologies after removing corrosion products were observed using scanning electronic microscopy (SEM, JSM-7500F) equipped with energy-dispersive X-ray spectrometry (EDAX) and the corrosion products on the specimen surface were analyzed by EDAX and X-ray diffraction (XRD, X'Pert PRO MPD).

3. RESULTS AND DISCUSSION

3.1 Corrosion rate

Fig. 3 shows the corrosion rate as a function of immersion time for all tested steels. With immersion, the steel corrosion rate immersed in low temperature (0 °C) seawater initially increased, and then slightly decreased, finally stabilizing at a high value (about 10~11 mg/(dm²·d)). Initially, chloride ions can directly interact with the base material as the main corrosion components [29-33], causing a corrosion reaction and leading to an increase in corrosion rate. Notably, the low temperature slowed the corrosion reaction, producing a lower corrosion rate than that observed in room temperature solution. Moreover, the slow corrosion reaction prevented the formation of a corrosion product film on the surface and loose corrosion deposits were formed instead, which did not adhere to the surface. The corrosion rate continuously increased after seven days of immersion. After 14 days of immersion, the corrosion rate decreased slightly because the loose corrosion deposits adhered to the surface and the deposits slightly reduced the corrosion rate. Eventually, the corrosion rate remained stable after immersion for 21 days. This can be attributed to reaching equilibrium between the formations and falling off of loose corrosion products. With the steel specimens immersed in room temperature seawater, the corrosion of steel initially increased, and then decreased after seven days, before finally stabilizing at about 4~5 mg/(dm²·d). Initially, chloride directly corroded the steel and the corrosion reaction was relatively high. After corrosion for seven days, the corrosion-produced film gradually formed on the surface of the steel, leading to a drop of corrosion rate. By extending the corrosion time, an intact and compact film formed on the steel; thus, inhibiting further corrosion. Cheng and his coworkers [34] reported that the corrosion rate of Q235B carbon steel was high at first immersion, then decreased gradually due to the protection of corrosion products, and fluctuated within a narrow range after long-time immersion. In this work, with longer immersion time, the corrosion rate showed a similar trend.

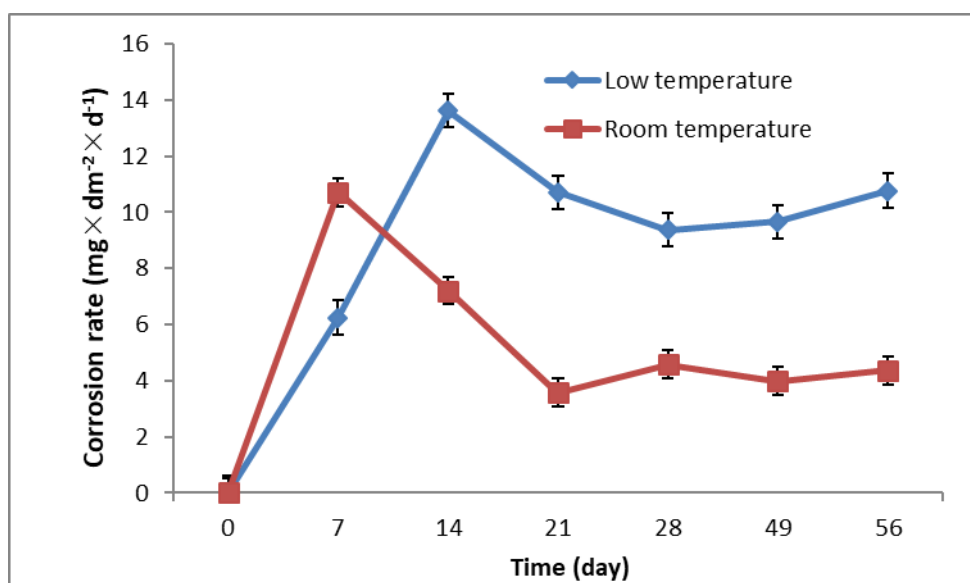


Figure 3. Time dependence of the EH40 steel corrosion rate in low temperature and room temperature artificial seawater over different immersion time intervals.

3.2 Impedance Measurements

EIS is a powerful, non-destructive electrochemical technique to study the interface reaction ability at the metal/film interface and the formation of corrosion products [35-37]. Figure 4 shows the impedance spectra of the steel in cold seawater after different immersion times. In the Nyquist plots (Fig. 4a), the diameters of the impedance loops gradually decreased for the first 21 days. After 21 days, the Nyquist spectrum consisted of one depressed capacitance loop, showing that the electrode is not a pure capacitor, caused by the inhomogeneity and unevenness of the electrode surface [38]. This result indicated that uneven and loose corrosion products formed on the steel surface contributed to the asymmetrical current distribution on the steel surface. The Bode impedance plot (Fig. 4b) illustrated that the logarithmic value of impedance decreased from ~ 2.9 to ~ 2.77 at the lowest frequency with immersion time. This result demonstrates the decrease in corrosion resistance resulting from a lack of protective corrosion film formation on the steel surface. From the Bode angle plots (Fig. 4c), only one peak maximum was observed at the low frequency range. No peak maxima appeared at the high frequency range, which was attributed to the lack of protective oxide film formation on the specimen surface. Notably, the characteristic phase maxima yielded only one time constant [39] for the steel samples in the cold seawater.

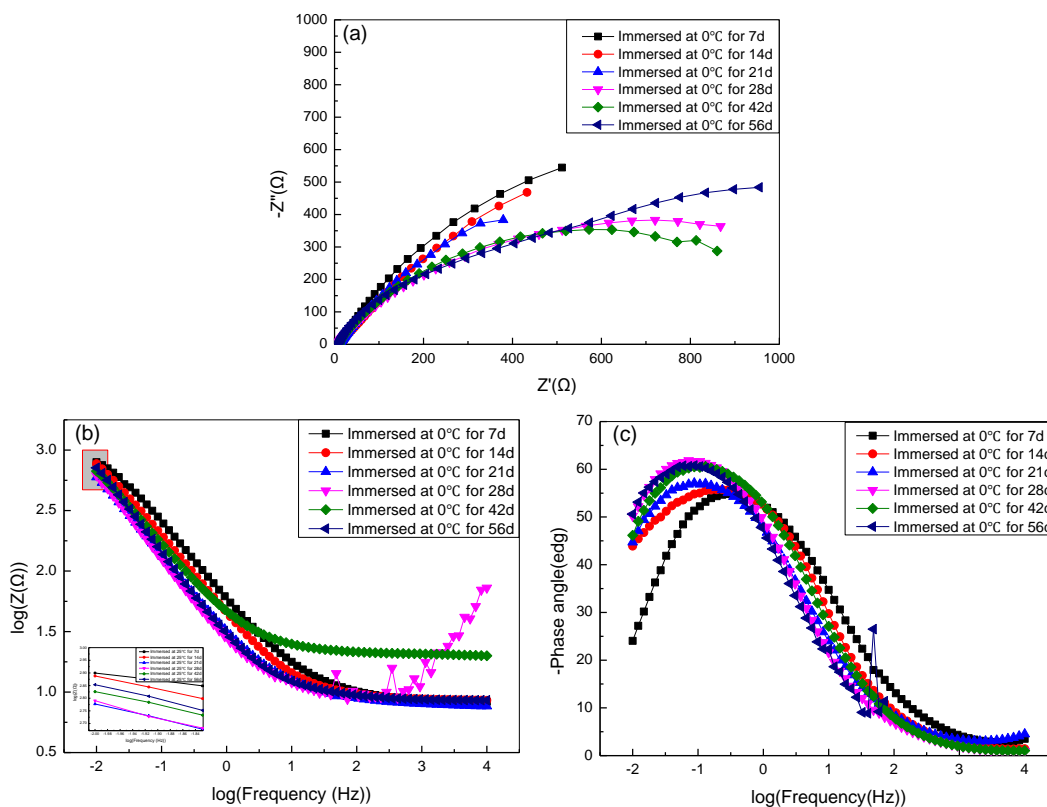


Figure 4. Impedance spectra of the EH40 steel in low temperature (0 °C) seawater for different immersion times: (a) Nyquist plots, (b) Bode impedance plots, and (c) Bode angle plots.

Fig. 5 illustrates the impedance spectra of the EH40 steel in room temperature artificial seawater. The diameters of impedance arcs in the Nyquist plots increased with time, indicating a decrease in the corrosion rates of the steel specimens. The Bode impedance plot (Fig. 5b) illustrates

that the logarithmic value of impedance varied from ~2.87 to ~3.04 at the lowest frequency with exposure time, indicating the formation of a protective oxide film, which increased the corrosion resistance of the steel. As shown in the Bode angled plots (Fig. 5c), one peak maxima appeared at the high frequency range from 28 to 56 days and the peak phase angles in the high frequency range gradually increased from ~55° to ~60° over time. These results suggest that the protective oxide film formed on the specimen surface leads to a decrease of corrosion rate.

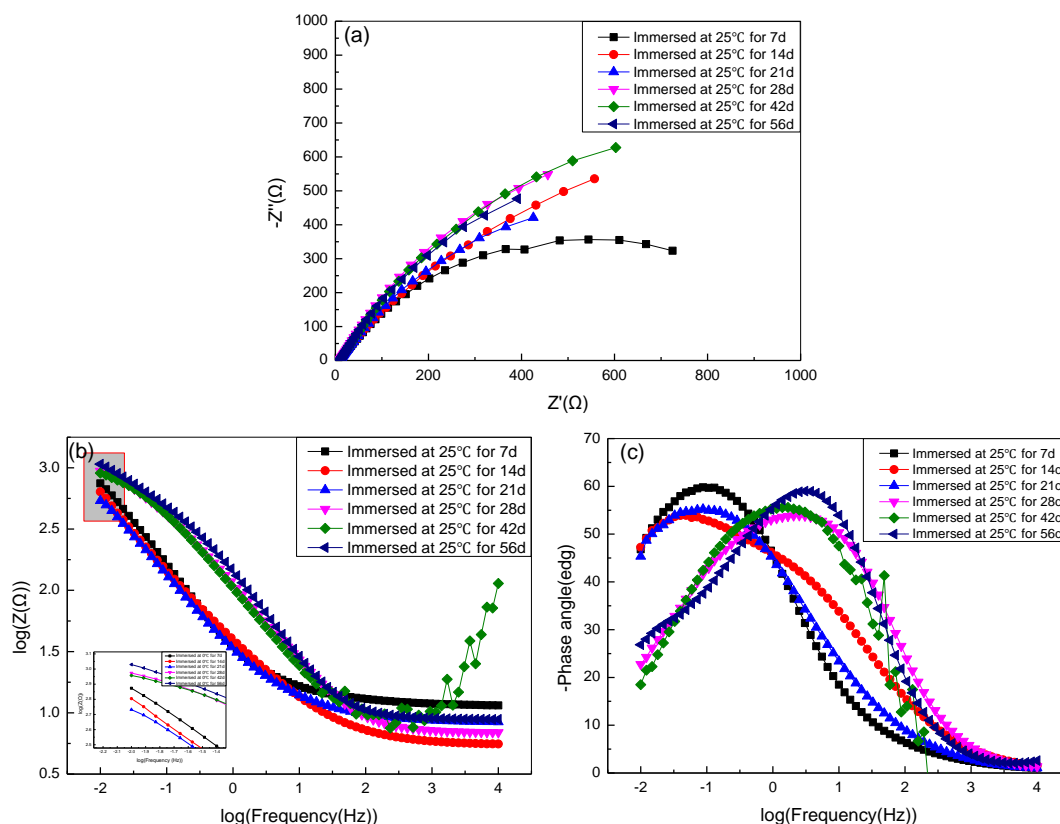


Figure 5. Impedance spectra of the EH40 steel in room temperature (25 °C) seawater for different immersion times: (a) Nyquist plots, (b) Bode impedance plots, and (c) Bode angle plots.

The steel corrosion characteristics in different temperature artificial seawater were further analyzed by one and two equivalent circuits (Fig. 6). Data were fitted with the built-in software of Autolab. In the equivalent circuits R_s represents the solution resistance; CPE_f and R_f represent the capacitance and resistance of the insoluble corrosion products formed during exposure, respectively; CPE_{dl} represents the double-layer capacitance at the surface of the electrolyte solution and the steel substrate; CPE_{dl} and CPE_f represent the constant phase angle elements used a capacitor substitute to compensate for a non-homogenous system; R_{ct} represents the charge transfer resistance; and Z_{CPE} represents the impedance of the constant phase element (CPE), as shown in formula (2), where ω represents the angular frequency and Z_0 and n represent positive integers.

$$Z_{CPE} = Z_0 \cdot (j\omega)^{-n}, \tag{2}$$

As shown in formula (2), $n = 1$ represents the ideal capacitor; $n = -1$ represents inductance, and $n = 0.5$ represents the Warburg impedance. Tables 2 and 3 list the fitting parameters of steel at different conditions. Usually, R_{ct} was used to characterize the corrosion rate and was inversely

proportional to the corrosion rate. When the steel was immersed in low-temperature solutions for 14 days, R_{ct} decreased with time due to the direct bare metal contact with the corrosion medium and no corrosion product formed on the metal surface [40-41], indicating an initial increase in corrosion rate.

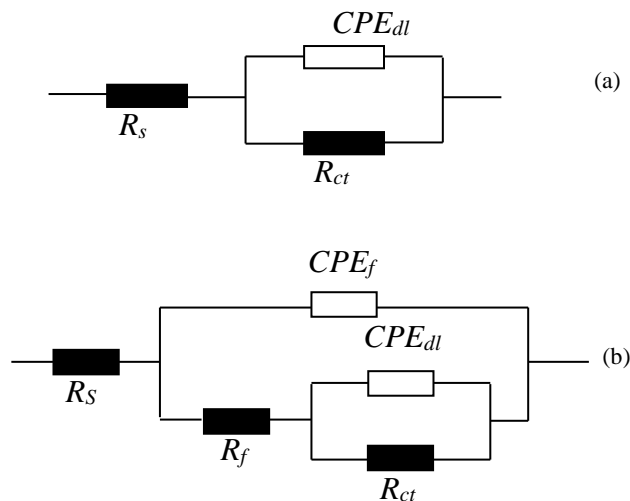


Figure 6. Two equivalent circuits used for fitting the impedance data of the steel specimens in artificial seawater at different temperature: (a) fitting data with only one capacitive loop and (b) fitting data with two capacitive loops.

After 14 days of immersion, R_{ct} slightly increased due to the formation of corrosion products, and then markedly decreased with increasing immersion time due to the propagation of stable, broad pits, which demonstrated that the corrosion rate increased after 21 days of immersion. The results were consistent with the pitting corrosion topography. The value of n_1 increased and reached 0.995 after 56 days of immersion, indicating that the capacitive character gradually increased. The resistance of oxide films, R_f are always 0, suggesting that no oxide film formed on the surface of the steel immersed in cold seawater. In contrast, for the room-temperature seawater, the R_{ct} of the steel initially decreased and then increased, indicating that the corrosion rate first increased and then decreased. The R_f increased with immersion time, indicating a gradual growth of oxide film in thickness and compactness over immersion time. The value of R_f reached as high as 328 Ω after 56-day immersion, which is notably higher than those of the other specimens. This was possibly caused by the oxide film. The n_2 values were above 0.7, which is indicative of the high homogeneity and compactness of layers, since the uniform and compact corrosion products film formed on the steel surface [42].

The corrosion behavior was further confirmed by analyzing the obtained open circuit potential (OCP) (Fig. 7). Based on the variation in the OCP with time (Figure 7), the trend of the OCP changed depending on the testing temperature. When the specimens were immersed in the cold artificial seawater, the OCP fluctuated slightly, demonstrating a slight fluctuation between positive and negative directions. This is mainly because the loose corrosion deposits fell off constantly, leading to the absence of the protective film on the specimen surface even pitting. Moreover, both the cathodic and anodic reactions affected the corrosion process at the later stages of immersion. These reactions can cause a shift of OCP in the negative direction and an increase in corrosion rate. For room temperature

immersion, the OCP of the specimen initially decreased and then increased. This is consistent with the presented corrosion rate and EIS results. The accumulation of corrosion deposits may cause a positive shift of OCP. As the protective corrosion film gradually forms and thickens, the corrosion rate decreases. Consequently, the OCP of the specimen shifts in the positive direction over time after 14 days of immersion.

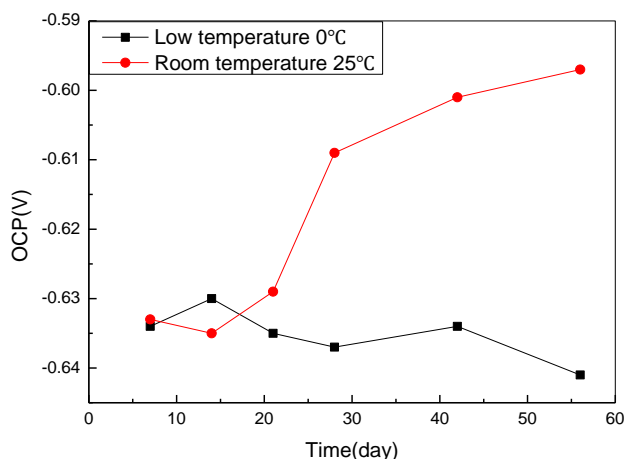


Figure 7. Time dependence of the open circuit potentials (OCPs) of the low temperature steel EH40 at 0 °C and 25 °C artificial seawater for different immersion times.

Table 2. Fitting parameters of EIS measurements of EH40 steel in cold artificial seawater for different days of immersion, respectively

T(days)	$R_s(\Omega)$	CPE_{dl}	n_1	$R_{ct}(k\Omega)$	CPE_f	n_2	$R_f(\Omega)$
7	8.48	4.89	0.689	2.39	---	---	---
14	8.63	6.82	0.692	2.08	---	---	---
21	8.00	10.0	0.684	2.16	---	---	---
28	8.65	7.43	0.726	1.70	---	---	---
42	8.22	10.2	0.995	1.56	---	---	---
56	10.0	11.5	0.995	1.38	---	---	---

Table 3. Fitting parameters of EIS measurements of EH40 steel in 25 °C artificial seawater for different days of immersion, respectively

T(days)	$R_s(\Omega)$	CPE_{dl}	n_1	$R_{ct}(k\Omega)$	CPE_f	n_2	$R_f(\Omega)$
7	9.31	8.71	0.723	2.54	---	---	---
14	5.53	9.10	0.596	2.53	---	---	---
21	8.70	10.3	0.651	3.39	---	---	---
28	6.88	1.54	0.496	2.40	1.59	0.733	100
42	8.47	27.2	0.683	2.88	---	---	---
56	8.84	2.82	0.423	3.34	1.31	0.821	328

3.3 Tafel Plot Tests

Tafel curve measurements are widely used to monitor corrosion potential and corrosion current density of a metal or an alloy exposed to corrosive environments and data plots can also be further quantitatively analyzed with the built-in software of the electrochemical workstation. Fig. 8 shows the Tafel curves of experimental steels immersed in artificial seawater solution at 25 °C and 0 °C after different exposure times. Table 4 and Table 5 show the analyzed data. From Fig. 8 (a) and Table 4, it can be seen that i_{corr} decreased with increasing immersion time from 19.60 to 1.65 A·cm⁻² for 56 days of immersion, which suggests that the corrosion rate of the steel decreased over time due to the formation of the corrosion products film protecting from further corrosion. E_{corr} , showed a slight positive shift from -0.823 V to -0.708 V after 56 days of immersion. The inhibition effect of the protective oxide film on the electrode reactions may be responsible for this positive shift. Anodic Tafel slope β_a increased with immersion time, indicating an increase in difficulty for electron transfer from the anodic site after the protective oxide film formation; however, cathodic Tafel slope β_c fluctuated with exposure time, showing no visible changing trends. These findings parallel the corrosion rate and the corrosion morphology results.

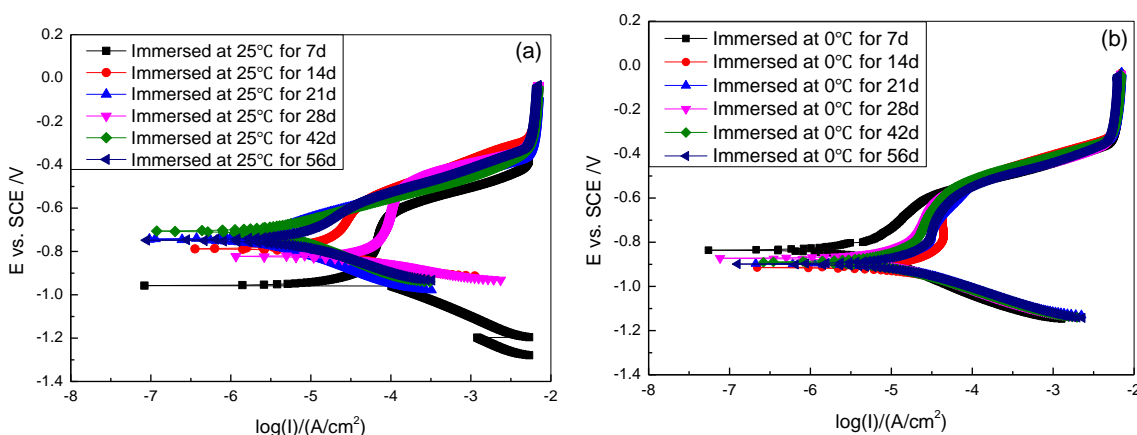


Figure 8. Tafel curves of the steel specimens in artificial seawater at low and room temperature after different exposure times: (a) corroded at 25 °C and (b) corroded at 0 °C.

Table 4. Fitting data of Tafel curves of the EH40 steel in the room temperature (25 °C) artificial seawater after different exposure times.

Exposure time(days)	β_c (mV·dec ⁻¹)	β_a (mV·dec ⁻¹)	E_{corr} (V)	i_{corr} (μA·cm ⁻²)
7	-440	40	-0.823	19.60
14	-801	95	-0.787	19.06
21	-193	142	-0.743	3.40
28	-298	81	-0.723	5.32
42	-101	142	-0.706	4.10
56	-36	136	-0.708	1.65

Table 5. Fitting data of Tafel curves of the EH40 steel in the low temperature (0 °C) artificial seawater after different exposure times.

Exposure time(days)	β_c (mV·dec ⁻¹)	β_a (mV·dec ⁻¹)	E_{corr} (V)	i_{corr} ($\mu\text{A}\cdot\text{cm}^{-2}$)
7	-344	112	-0.836	4.35
14	-741	184	-0.915	38.96
21	-88	77	-0.897	7.63
28	-122	71	-0.890	5.61
42	-215	88	-0.899	23.77
56	-117	85	-0.905	13.38

From Fig. 8(b) and Table 5, it is obvious that the low temperature conditions caused different corrosion characteristics for the steel samples compared to control specimens. i_{corr} first dramatically increased, and then decreased with exposure time, and increased to 13.38 A·cm⁻² after 56 days of immersion. These results demonstrate the fluctuation in the corrosion rate of the steel over time, due to the uneven protective oxide film formed on the specimen surface. Previous researches showed that the lower of corrosion potential of a material, the easier it corrodes [43]. E_{corr} of steel in low-temperature seawater shifted from -0.836 to -0.905 V after 56 days of immersion, indicating an acceleration of the corrosion rate. The Tafel slope of cathodic branches β_c decreased with time from -344 mV·dec⁻¹ to -177 mV·dec⁻¹, indicating an improvement of reaction kinetics for the cathodic reaction over exposure time.

3.4 Surface Morphology

Fig. 9 shows the surface topography of the steel after different exposure times during the 56-day period at cold environments. After 14 days of immersion, corrosion product patches distributed on the steel surface. For 28 days of immersion, the corrosion patches expanded and uneven corrosion products covered the surface of the sample area. As an extension of immersion time, the sample areas were covered by uneven corrosion patches and loose corrosion deposits.

Figure 10 shows the corresponding SEM pictures after acid-pickling removal of the corrosion products from the corrosion coupons.

Based on Fig. 9, after 56 days of immersion, the localized corrosion became increasingly severe and both uniform corrosion and local corrosion were observed (especially pitting corrosion). The size of corrosion pits was about 2~3 μm for the first seven days of immersion and then, the size of corrosion pits gradually enlarged and reached about 25 μm on day 28. For the next period of immersion, the size of corrosion pits did not increase continuously. However, uniform corrosion occurred after 28 days of immersion and pitting size gradually increased with initial immersion time.

In comparison, Figure 11 shows the surface topography of the steel after different exposure times at 25 °C. After seven days of exposure, scattered corrosion products were clearly observed on the specimen surface and were heterogeneous and loose (Fig 11a). After 28 days of exposure, a denser layer on the alloy surface was detected (Fig. 11c).

The corrosion product plating on the steel surface was uniform and compact with increasing immersion time, and after 56 days of immersion, a thick corrosion product layer had formed on the specimen. After removing the corrosion products, uniform corrosion was mainly observed on the surface (Fig. 12).

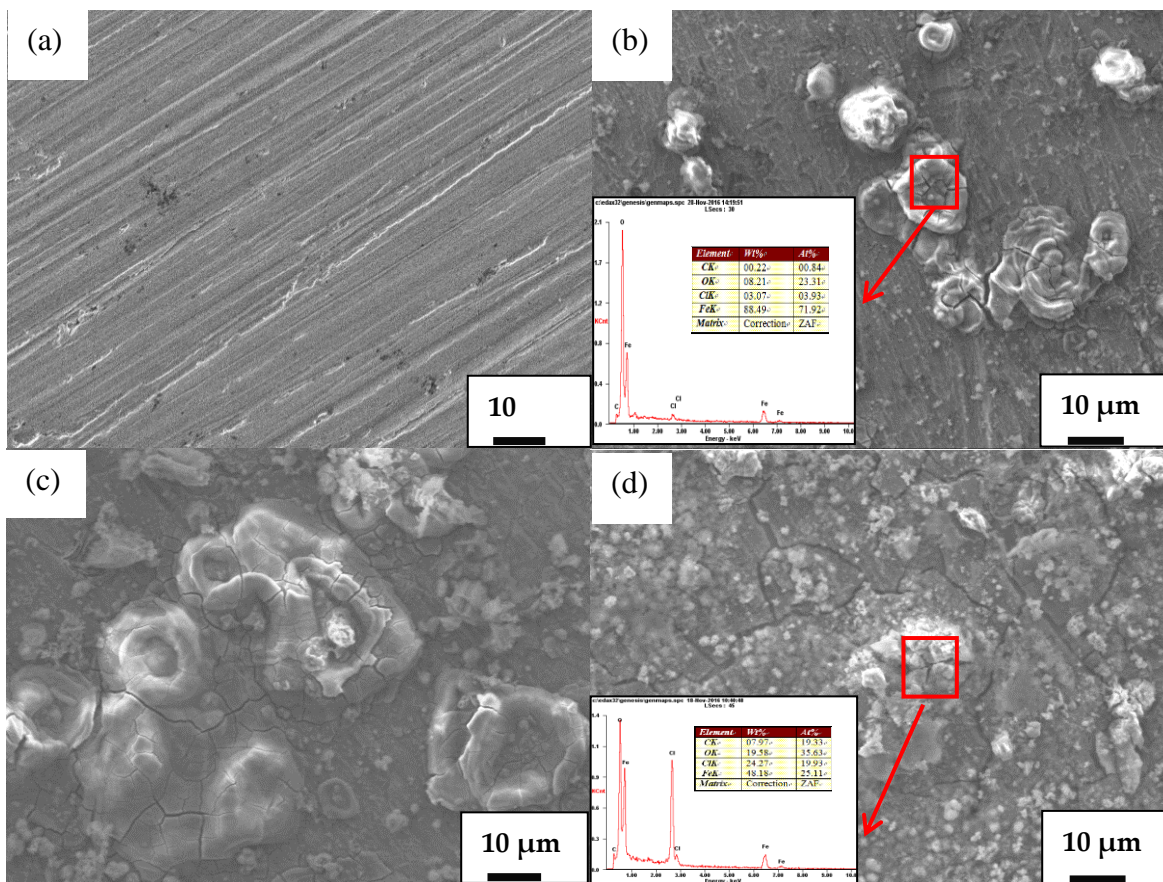
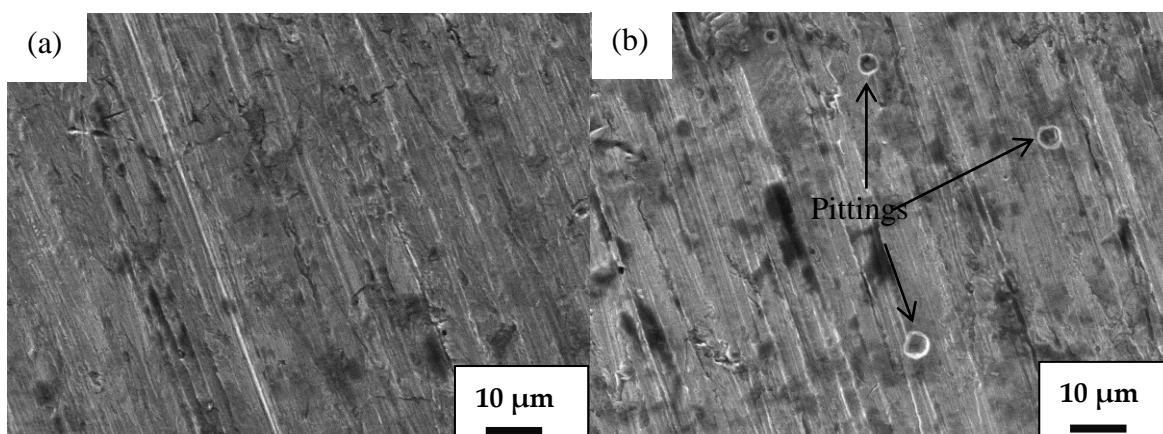


Figure 9. SEM images and corresponding EDS spectra of specimens after different immersion times in cold seawater (0 °C). (a) Original sample, (b) 14 d, (c) 28 d, and (d) 56 d.



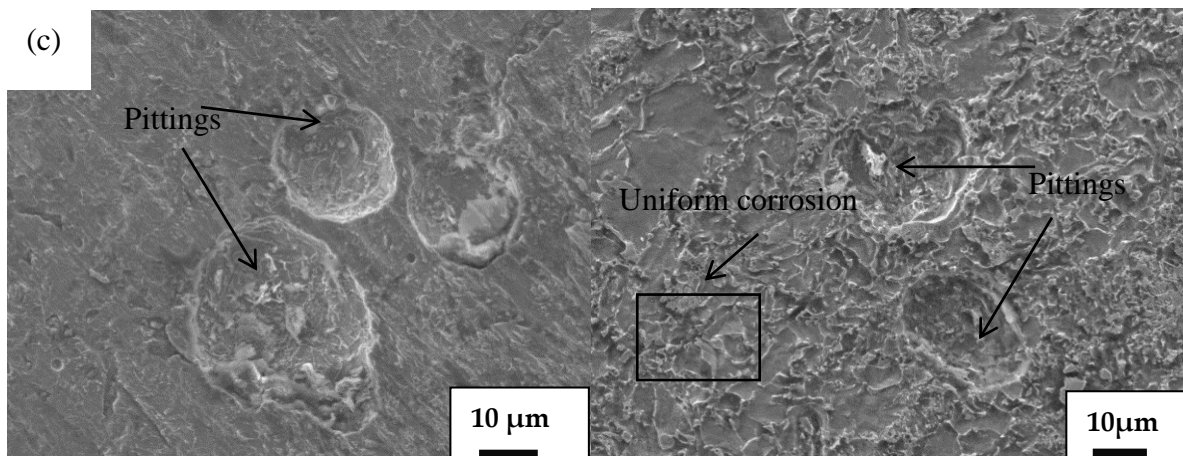


Figure 10. Corresponding SEM topography of samples after removal of the corrosion products for 7, 14, 42, and 56 days of immersion, respectively.

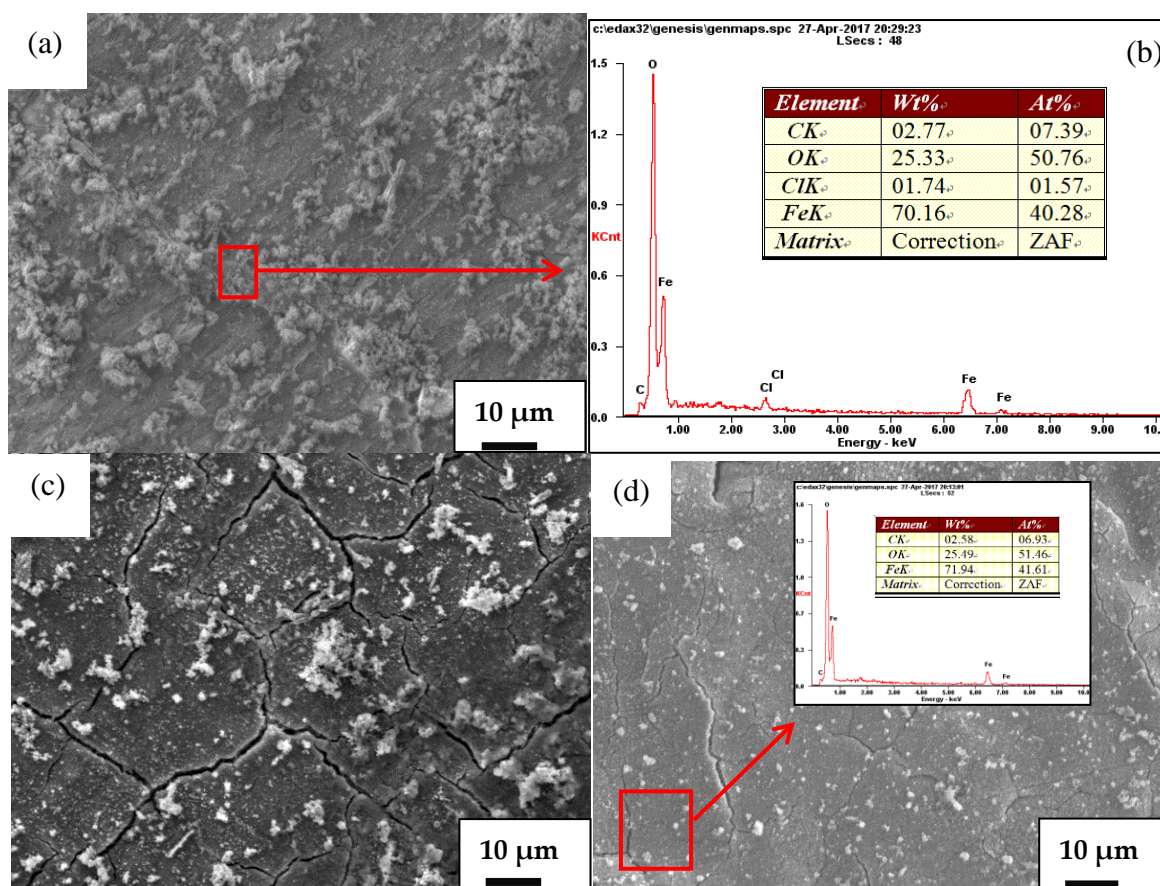


Figure 11. SEM images and corresponding EDS spectra of specimens after different immersion times at room temperature (25 °C). (a) Original sample, (b) 14 d, (c) 28 d, and (d) 56 d.

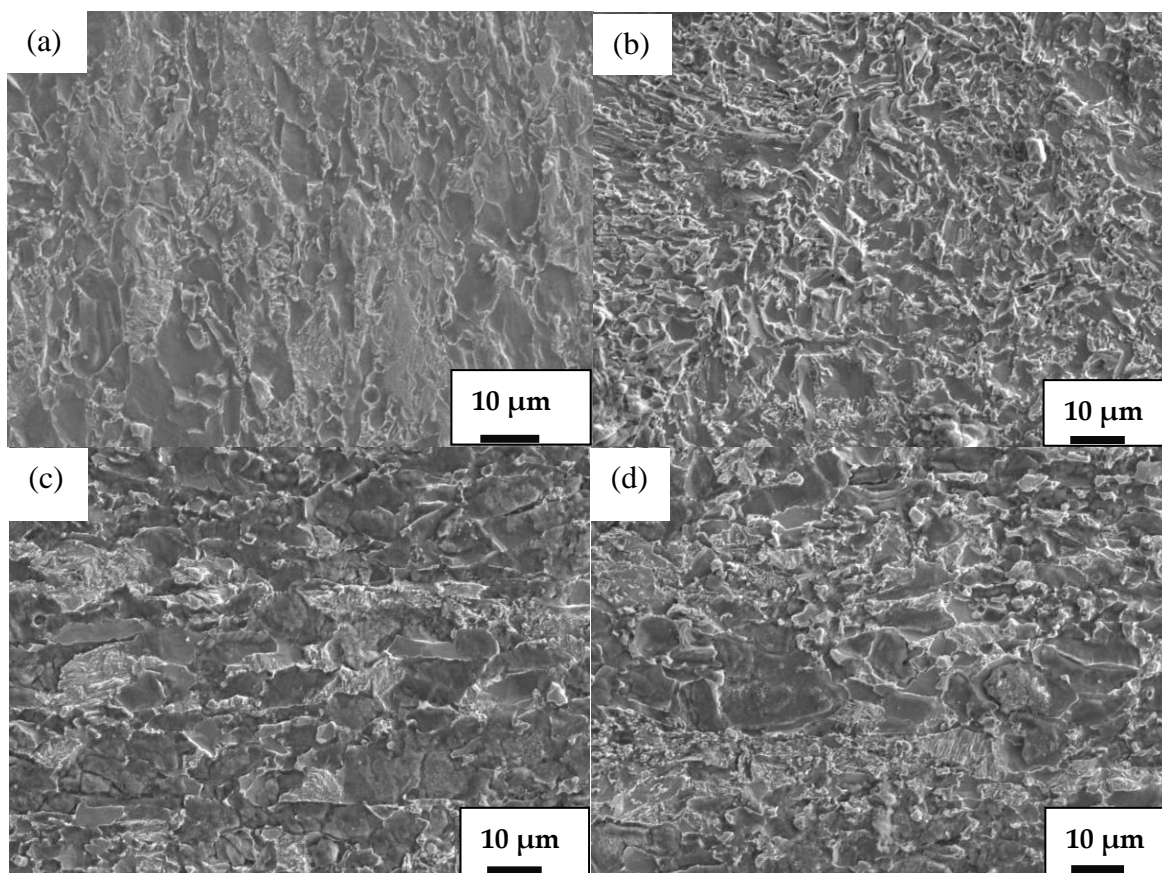


Figure 12. Corresponding SEM topography of samples after removal of the corrosion products for 7, 28, 42, and 56 days of immersion, respectively.

3.5 Corrosion Products Analysis

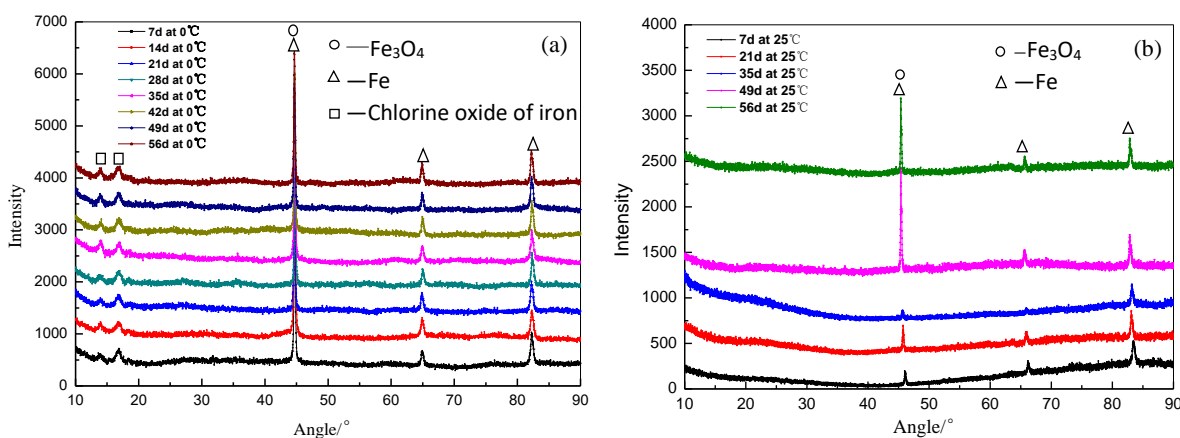


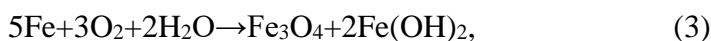
Figure 13. XRD patterns of the corrosion products on the EH40 steel immersed in artificial seawater over with different times: (a) Low temperature (0 °C) and (b) room temperature (25 °C).

EDS and XRD were employed to determine the composition and chemical states of the corrosion products. The EDS results for corrosion samples over different time intervals at 0 °C show

less oxygen and more chlorine compared to samples taken at 25 °C. For the products produced at 0 °C, the primary elements were Fe and Cl with trace amounts of O. Therefore, the precipitates were mainly chlorine oxide of iron and a trace amount of iron oxides. At 25 °C, the main elements in the products were Fe and O with trace amounts of Cl. These results suggest that the corrosion products formed in 25 °C artificial seawater mainly consist of iron oxides. Fig. 13 illustrates the XRD patterns of corrosion products on the steel surface after different immersion times at 0 °C and 25 °C in artificial seawater. Based on these results, the precipitates formed on the steel surface immersed at cold seawater mainly consisted of $\text{Fe}(\text{Cl}_x\text{O}_y)$ and Fe_3O_4 . While the corrosion products on the specimens corroded in 25 °C seawater were primarily Fe_3O_4 , after 35 days, the content of iron oxides increased with increasing immersion time.

3.6 Corrosion Mechanism Analysis

Normally, the higher the temperature, the more likely metal is to corrode. However, in the long-term immersion experiment, many factors affect the corrosion. In this research, the corrosion rate was higher in room temperature seawater during the first seven days of immersion, which was in accordance with the normal results. However, chloride ions form an important factor that affect the pitting, which plays a decisive role in the later corrosion. Cl^- is an aggressive ion that can destroy the formation of oxide layers [44] and easily pass through the corrosion produced film. The main reactions are as follows:



Due to the slower reaction rate of (3) at low temperature seawater, the protective oxide film did not form on the specimen surface, allowing Cl^- to pass through the corrosion product and to accumulate on the surface. $\text{Fe}(\text{ClO})$ precipitation is therefore promoted in extreme cold seawater by reaction (4). When the enriched Cl^- concentration exceeds a threshold in a local region of the specimens [45], new pitting corrosion is possibly initiated. Supposedly, the scale loose $\text{Fe}(\text{ClO})$ cannot provide protection for steel substrate after prolonged immersion. Consequently, the steel surface suffers from continuous attack of corrosive substances, causing an increase in pitting size in artificial seawater at extreme cold condition. At room temperature, reaction (3) occurred quickly and a uniform and compact iron oxide film soon formed on the steel surface protecting the steel from further erosion.

However, previous research indicated that the hydrogen evolution potential in low-temperature seawater was lower than that in room-temperature seawater [27]. Hydrogen induced cracks were likely to occur. In this work, when the EH40 steel was immersed in extreme cold seawater, the crack occurred and extended, thus promoting the initiation of eventual pitting corrosion [46]. Moreover, the local corrosion and deposits could not prevent the diffusion of Cl^- into the crack of the steel matrix, leading to pitting growth and extension. Overall, EH40 steel is likely to suffer from pitting in low-temperature seawater. However, in room-temperature seawater, hydrogen induced cracks and uniform corrosion did not occur.

4. CONCLUSIONS

The corrosion behavior of EH40 in an artificial seawater medium at both low temperature and room temperature conditions was investigated via mass loss, SEM/EDS, XRD, and electrochemical techniques. The main conclusions can be summarized as follows:

1. For both temperatures, the corrosion rate of steel specimens initially increased and then decreased; however, the corrosion rate at low temperature was higher than at room temperature after 21 days immersion because no protective corrosion products film formed on the steel surface.
2. In the low-temperature seawater, the corrosion product layer formed on the steel surface was loose and porous, which could not prevent the corrosion of steel from the corrosion medium. The main corrosion products consisted of $\text{Fe}(\text{Cl}_x\text{O}_y)$ and Fe_3O_4 .
3. The specimens subjected to extremely cold artificial seawater conditions mainly exhibited pitting and pitting size gradually grew to 25 μm due to the Cl^- passing through the loose corrosion product layer and continuously enriching the surface. For the samples in room temperature artificial seawater, a protective corrosion produced-film formed on the surface, which was mainly composed of Fe_3O_4 .

In summary, the modified high strength ocean engineering structural steel EH40 showed pitting in low temperature seawater, which can contribute to accelerated corrosion processes; therefore, it is necessary to improve the anti-corrosion property of EH40 steel in extremely cold seawater.

ACKNOWLEDGMENTS

The authors acknowledge the financial support of the National Key Research and Development Program (No. 2016YFB0300700), the National Natural Science Foundation (Nos. 51609133 and 5162195), and the China Postdoctoral Science Foundation (No. 2017M620153).

References

1. M.W. Downey, *Encyclopedia Energy*. (2004) 549.
2. V. D. Kaminskii, O. I. Suprunenko, V. V. Suslova, *Russ. Geol. Geophys.* 52 (2011) 760.
3. R. F. Aguilera, R. D. Ripple1, *Appl. Energy*. 96 (2012) 387.
4. Q. Guan, H. Z. An, *Appl. Energy*. 203 (2017) 154.
5. E. R. Camp, T. E. Jordan, M. J. Hornbach, C. A. Whealton, *Geothermics*. 71 (2018) 187.
6. H. J. Wang, F. Ma, X. G. Tong, Z. D. Liu, X. S. Zhang, Z. Z. Wu, D. H. Li, B. Wang, Y. F. Xie, L. Y. Yang, *Pet. Explor. Dev.* 43 (2016) 925.
7. A.E.Kontorovich, M.I.Epov, L.M.Burshtein, V.D.Kaminskii, A.R.Kurchikov, N.A.Malyshev, O.M.Prishepa, A.F.Safronov, A.V.Stupakova, O.I.Suprunenko, *Russ. Geol. Geophys.* 51 (2010) 3.
8. A.M.Brekhuntsov, I.I.Nesterov Jr., L.A.Nechiporuk, *Russ. Geol. Geophys.* 58 (2017) 362.
9. Y. K. Yang, A. Marshak, M. Han, S. P. Palm, D. J. Harding, *J. Quant. Spectrosc. Radiat. Transfer*. 188 (2017) 159.
10. S. H. Faria, I. Weikusat, N. Azuma, *J. Struct. Geol.* 61 (2014) 2.
11. B. Thurairajah, S. M. Bailey, D. E. Siskind, C. E. Randall, M. J. Taylor, J. M. Russell, *J. Atmos. Sol. Terr. Phys.* 104 (2013) 224.
12. X. L. Liu, G. Falcone, C. Alimonti, *Energy*. 142 (2018) 346.
13. M. Setiyo, S. Soeparman, N. Hamidi, S. Wahyudi, *Int. J. Refrig.* 82 (2017) 227.

14. J. J. Bao, Y. Lin, R. X. Zhang, N. Zhang, G. H. He, *Appl. Therm. Eng.* 126 (2017) 566.
15. Z.X. Sun, F.Q. Xu, S.J. Wang, J.P. Lai, K. Lin, *Energy*. 139 (2017) 380.
16. K. Ravi, J.P. Bhasker, E. Porpatham, *Fuel*. 205 (2017) 71.
17. H.S. Kim, C.J. Lee, K.S. Choi, M.C. Kim, *Int. J. Nav. Arch. Ocean.* 3 (2011) 208.
18. Y.F. Yang, J.D. Scantlebury, E. Koroleva, *Corrosion*. 68 (2012) 432.
19. D.Y. Yu, J.T. Tian, J.H. Dai, X. Wang, *Corrosion*. 70 (2014) 329.
20. V.A. Katkar, G. Gunasekaran, *Corrosion*. 72 (2016) 400.
21. H. Song, H. Shin, Y. Shin, *Ocean Eng.* 122 (2016) 278.
22. S.Y. Hwang, Y. Kim, J.H. Lee, *J. Mater. Process. Technol.* 229 (2016) 349.
23. C.J. Wen, C.W. Wan, B.A. Gyu, U.P. Jeong, *Mater. Des.* 51 (2013) 415.
24. Z.J. Xia, Z.M. Miao, J. Zhu, *Steel Constr. Des. Res.* 30 (2015) 32.
25. T.G. Park, J.M. Kim, H.Y. Yoon, J.H. Lee, J.C. Won, K.K. Ho, *Korean J. Met. Mater.* 48 (2010) 1021.
26. P.Y. Zhang, C.R. Gao, F.X. Zhu, *Acta Metall. Sinica*. 48 (2012) 264.
27. L. Zhang, M. Du, Y. Li, *Corrosion*. 68 (2012) 713.
28. ISO8407, *Corrosion of metals and alloys—Removal of corrosion products from corrosion test specimens*, ISO, (2009 (E.)) Switzerland
29. L.B. Niu, K. Nakada, *Corros. Sci.* 96 (2015) 171.
30. Y.S. Wang, G.X. Wu, L. He, P.M. Singh, *Corrosion*. 72 (2016) 628.
31. C. Ornek, X.L. Zhong, D.L. Engelberg, *Corrosion*. 72 (2016) 384.
32. S. H. Mameng, R. Pettersson, J. Y. Jonson, *Mater. Corros.* 68 (2017) 272.
33. G.S. Peng, K.H. Chen, H.C. Fang, H. Chao, S.Y. Chen, *Mater. Corros.* 61 (2010) 783.
34. Q.L. Cheng, B. Tao, L.Y. Song, W.H. Zhang, X.Y. Liu, W.H. Li, B.R. Hou, Q.Z. Liu, *Corros. Sci.* 111 (2016) 61.
35. Q. Cheng, S. Song, L. Song, B. Hou, *J. Electrochem. Soc.* 160 (2013) 380.
36. S.J. Yuan, Amy M.F. Choong, S.O. Pehkonen, *Corros. Sci.* 49 (2007) 4352.
37. Q. Cheng, Z. Chen, *Int. J. Electrochem. Sci.* 8 (2013) 8282.
38. W.S. Tail, *Prog. Org. Coat.* 26 (1995) 73.
39. C.Q. Ye, R.G. Hu, S.G. Dong, X.J. Zhang, R.Q. Hou, R.G. Du, C.J. Lin, J.S. Pan, *J. Electroanal. Chem.* 688 (2013) 275.
40. X.Y. Lou, P.M. Singh, *Electrochim. Acta.* 56 (2011) 1835.
41. C.M. Pradier, P. Bertrand, M.N. Bellon-Fontaine, C. Compère, D. Costa, P. Marcus, C. Poleunis, B. Rondot, M.G. Walls, *Surf. Interface Anal.* 30 (2000) 45.
42. F. Mansfeld, G. Liu, H. Xiao, C.H. Tsai, B.J. Little, *Corros. Sci.* 36 (1994) 2063.
43. C. Kato, B.G. Ateya, J.E. Castle, H.W. Pickering, *J. Electrochem. Soc.* 127 (1980) 1897.
44. C. D. Waard, U. Lotz, D. Milliams, *Corrosion*, 47 (1991) 976.
45. V. Soulie, F. Lequien, F.F. Gomes, G. Moine, D. Feron, P. Prene, H. Moehwald, T. Zemb, H. Riegler, *Mater. Corros.* 68 (2017) 927.
46. H.D. Li, Y.H. Dong, Y.Y. Shen, X.T. Chang, D.S. Wang, X.F. Li, Y.S. Yin, *Int. J. Electrochem. Sci.*, 12 (2017) 11077.